Ozone Flux-Based Response Functions for Visible Foliar Injury and Photosynthetic Traits in a Bioindicator Species, *Viburnum lantana* L.

Elena Marra , Barbara Baesso Moura * , Elena Paoletti , Andrea Viviano , Jacopo Manzini , Ryoji Tanaka , Yasutomo Hoshika

Posted Date: 15 May 2026

doi: 10.20944/preprints202605.0989.v1

Keywords: ozone visible foliar injury; photosynthesis; bioindicator; wayfaring tree; stomatal ozone flux

 doi:10.20944/preprints202605.0989.v1

Article

Ozone Flux-Based Response Functions for Visible Foliar Injury and Photosynthetic Traits in a Bioindicator Species, *Viburnum lantana* L.

Elena Marra [1], Barbara Baesso Moura [2,3,*], Elena Paoletti [2,3], Andrea Viviano [2], Jacopo Manzini [4], Ryoji Tanaka [5] and Yasutomo Hoshika [2,3]

[1] Department of Forest Biomaterials and Technology (SLU), Swedish University of Agricultural Sciences, 907 36 Umeå, Sweden
[2] Institute of Research on Terrestrial Ecosystems (IRET), National Research Council of Italy (CNR), Via Madonna del Piano, I-50019 Sesto Fiorentino, Italy
[3] NBFC, National Biodiversity Future Center, Palermo 90133, Italy
[4] Department of Agricultural, Food, Environmental and Forestry Science and Technology (DAGRI), University of Florence, Piazzale delle Cascine, 18, 50144 Firenze, Italy
[5] Institute of Global Innovation Research, Tokyo University of Agriculture and Technology, Fuchu, Tokyo, 183-8509, Japan
* Correspondence: barbara.baessomoura@cnr.it

Abstract

Tropospheric ozone (O_3) is a phytotoxic air pollutant that can impair visible foliar injury (O_3 VFI) and reduces photosynthesis in sensitive forest species. *Viburnum lantana* L. has been widely used as an in situ bioindicator of O_3 pollution in mountainous areas of Europe; however, field-observed O_3-induced VFI as well as critical levels (CLs) established to protect forests, have not been validated. This study validated field-observed O_3 effects in *V. lantana* through experiments carried out in a Free-air O_3 eXposure infrastructure (FO_3X) and determined which O_3 metric (exposure-based—AOT40 or flux-based—POD_1) best explains O_3 effect on leaf physiology and VFI. *V. lantana* saplings were subjected to ambient air (AA) conditions and elevated O_3 levels at 1.5× and 2.0× AA. Throughout the experimental period (T1: 2-month and T2: 3.5-month O_3 exposure) measurements were taken for the Plant Injury Index (PII), light-saturated net photosynthetic rate (A_{sat}), stomatal conductance (g_s), leaf color index (SPAD), and the maximum photochemical efficiency of photosystem II (Fv/Fm). O_3 VFI was first observed in 2.0× after 16 days. As a result, O_3 treatment influenced PII, which was significantly higher in the 2.0× (9.06 ± 3.24) than in the 1.5× and AA treatments (1.31 ± 0.62 and 1.29 ± 0.71) at T2. The A_{sat}, SPAD, and F_v/F_m were significantly affected by O_3 treatments; no significant difference in g_s was found. POD_1 better explained variability in O_3 VFI and physiological parameters, with CLs proposed for *V. lantana* of 1.61 mmol m^{-2} and 1.22 mmol m^{-2} for a 4% reduction of A_{sat} and g_s, and a CL of 7.82 mmol m^{-2} for the onset of O^3 VFI.

Keywords: ozone visible foliar injury; photosynthesis; bioindicator; wayfaring tree; stomatal ozone flux

1. Introduction

Tropospheric ozone (O_3) is an oxidative atmospheric pollutant that negatively affects forest health. Despite regulatory efforts to reduce precursor emissions, O_3 concentrations across much of Europe continue to exceed the thresholds established for protecting ecosystems [1,2].

Upon entry into the leaves via the stomata, O_3 interacts with the mesophyll, triggering production of reactive oxygen species (ROS), which subsequently cause physiological impairment, visible foliar injury (O_3 VFI), and finally growth loss [3–6] while leaf phenotypic plasticity modulates

 doi:10.20944/preprints202605.0989.v1

plant sensitivity [7]. To investigate tree responses to O_3, several metrics have been developed, including the exposure-based index Accumulated Exposure Over a Threshold of 40 ppb (AOT40) [8]. However, flux-based indices, such as the phytotoxic O_3 dose above a flux threshold of Y nmol m^{-2} s^{-1} (POD_Y), have been proven to be more reliable [9] and account for the actual O_3 dose determined by cumulative O_3 uptake over the growing season [10].

O_3 VFI serves as a forest-health biomarker within monitoring initiatives, e.g., the International Co-operative Program on assessment and monitoring of air pollution effects on Forests (ICP Forests) [11]. This is because the O_3 VFI assessment is practical for evaluating O_3 impact on forests in the field without specialized equipment, making it suitable for long-term monitoring. Therefore, scientific efforts have been made to establish O_3 Critical Levels (CLs) for forest protection based on the assessment of O_3 VFI for some dominant tree species (e.g., *Fagus sylvatica* L., *Pinus halepensis* Mill., *Picea abies* L. Karst.) [12,13] and other forest tree or shrub species (e.g., *Betula pendula* Roth, *Larix decidua* Mill., *Populus tremula* L., *Salix caprea* L., *Rubus sp*., *Vaccinium myrtillus* L.) [14]. However, validation of O_3 VFI using manipulative experiments is still required to establish an appropriate CL for forest protection [15].

In the last decades, *Viburnum lantana* L. has been proposed as an in situ bioindicator of O_3 damage due to its foliar sensitivity and wide distribution in European forests. Field studies in the Italian Alps found "O_3-like" VFI (red stippling and leaf reddening), which was correlated with high O_3 levels (AOT40 > 30 ppm h), though symptom severity also reflected microclimatic conditions, indicating that the CL for O_3 VFI in this species is around 12 ppm h AOT40 [16]. Follow-up research confirmed these patterns, highlighting inter-annual variability likely linked to climate-driven differences in O_3 uptake [17]. Long-term monitoring through the ViburNeT network [18,19] further supported these findings, documenting a consistent relationship between regional O_3 concentrations and O_3 VFI frequency in *V. lantana*, with 20.7% to 50.6% of individuals exhibiting O_3 VFI frequency, depending on the year. More recently, Faralli et al. [20] demonstrated that symptom severity showed a significant association with lower specific leaf area (SLA) and higher trichome density, especially under high light exposure and in the upper canopy. These findings, although valuable, are based on field observations, where site-specific susceptibility of *V. lantana* to local environmental conditions can influence stomatal O_3 uptake and thus alter the response to O_3. To date, there has been no study evaluating O_3 damage to *V. lantana* on the basis of stomatal O_3 flux. Therefore, to fully understand and validate its biomonitoring potential for setting the biological O_3 standard, it is essential to investigate the species' O_3 response under controlled conditions, such as through Free-Air Controlled Exposure (FACE) systems, aiming to establish a flux-based CL for this bioindicator species.

The present study induced O_3 VFI in the forest bioindicator species *V. lantana* plants exposed at the Free-Air O_3 eXposure (FO_3X) facility to compare these observations with those reported previously at natural forest sites (e.g., Gottardini et al. [16]), with the primary aim of validating field-based observations under controlled conditions.

In addition, the study aimed to determine which indices between exposure-based (AOT40) and flux-based (POD_1) more accurately capture the effects and incidence of O_3-related VFI and photosynthetic impairment in the bioindicator species *V. lantana*.

2. Materials and Methods

2.1. Experimental Site and Plant Material

Ozone exposure experiments were conducted at the FO_3X facility situated within the experimental garden of the National Research Council of Italy (Sesto Fiorentino, Italy: 43°48′59″ N, 11°12′01″ E, 55 m above sea level). The fumigation system details are provided in Paoletti et al. [21]. In December 2023, three-year-old *Viburnum lantana* L. saplings, raised in Santa Giustina in Colle (Padova, Veneto, Italy), were obtained from a local nursery (Vivai Guagno). At the time of transplantation, the plants, grown in 18 cm pots, had an average height of 74.7 cm and a stem diameter of 13.5 mm. Each plant was transplanted into a 9 L plastic pot (24 cm diameter) containing

 doi:10.20944/preprints202605.0989.v1

a uniform mixture of sand, peat, and soil in equal parts (v:v:v). This substrate composition was selected to ensure adequate drainage, nutrient availability, and root aeration during the subsequent growth period. All plants were watered daily to prevent water stress. From 17th May to 16th October 2024 (152 days), three levels of O_3 concentration treatments (ambient O_3 concentration [AA], 1.5 times ambient O_3 concentration [1.5×], and doubled ambient O_3 concentration [2.0×]) were applied using three replicated plots (dimension of 5 m × 5 m × 2 m) and 1- 2 plants were assigned for each plot.

The average hourly O_3 concentrations in the AA, 1.5×, and 2.0× treatments were 38.0 ppb, 48.6 ppb, and 61.3 ppb, respectively. Figure 1 shows the seasonal patterns of solar irradiance, precipitation, and mean daily temperature, based on hourly meteorological data collected throughout the growing season.

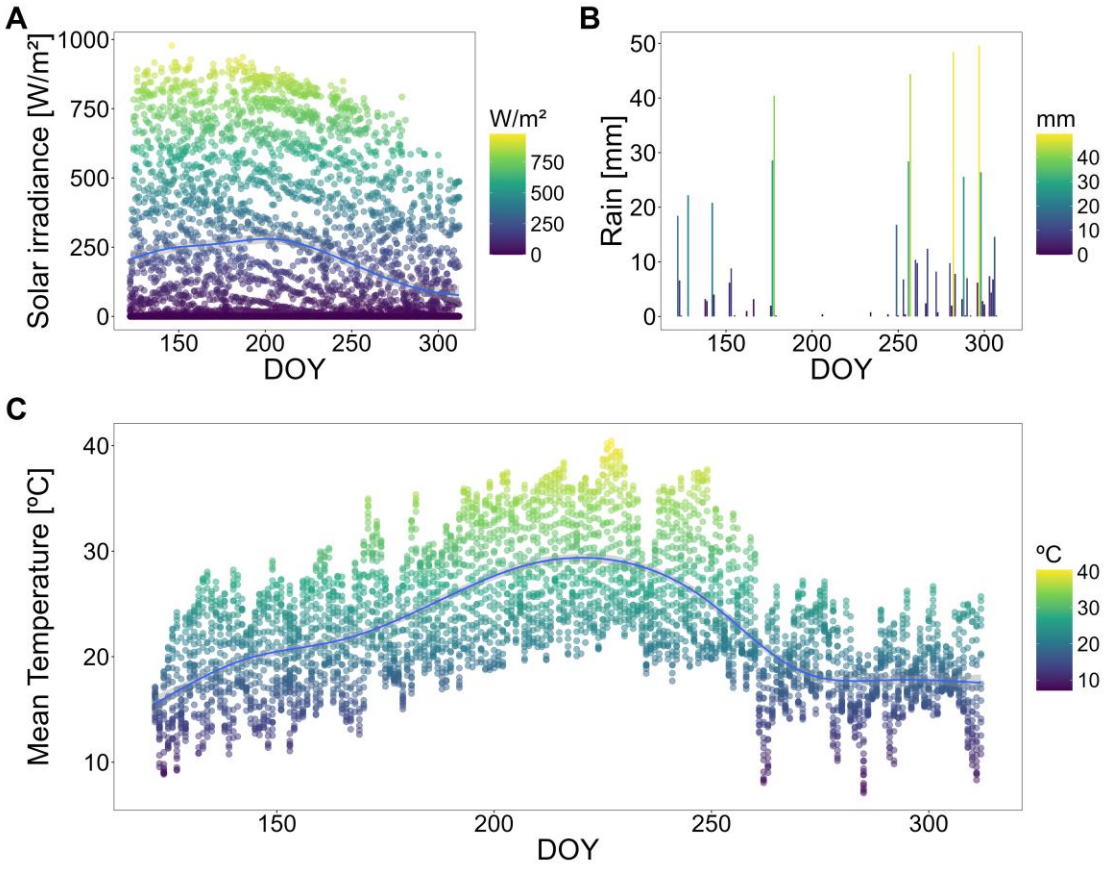

Figure 1. Seasonal patterns of solar irradiance, precipitation, and temperature by day of year (DOY) during the experiment. Color gradients illustrate the magnitude of each variable, with daily rainfall totals (**B**), average hourly data shown as dots, and monthly averages depicted as smoothed lines for solar irradiance (**A**) and mean temperature (**C**).

2.2. Assessment and Quantification of Visible Foliar Injury

Visible foliar injury attributable to O_3 was monitored at 2- or 3-week intervals throughout the exposure period. Assessments were carried out independently by two trained observers with ICP Forests Intercalibration experience [11]. For each plant, we recorded the proportion of leaves showing symptoms (SL) and, within symptomatic leaves, the mean affected leaf area (SA), using a ×10 hand lens and published photographic references [22]. To quantify the injury at the plant level, the Plant Injury Index (PII) was calculated by combining the two parameters [22,23] as follows:

$$PII = \frac{(SL \times SA)}{100} \qquad (1)$$

To describe, classify, and standardize O_3 VFI, color composition was assessed based on the methodology suggested by Moura et al. [15]. Three pictures showing a range of injuries (expert visual

 doi:10.20944/preprints202605.0989.v1

assessment from 0 to 70% SL) were taken under natural lighting conditions, all on the same day (9–10 a.m.), using a digital camera (Cyber-shot DSC-H300, Sony, Tokyo, Japan). The photos were combined into a single RGB figure, subsequently processed using the indexed color mode. Following this, both a Local (Perceptual) and a 64-colour image were produced. Subsequently, all the tissue exhibiting greenish and the vein-related colors were extracted from the image, leaving only potential O_3 VFI colors visible [15].

2.3. Assessment of Photosynthetic Parameters

Measurements of photosynthetic parameters (i.e., SPAD, chlorophyll a fluorescence, and leaf gas exchange) were conducted three times (time zero—T0: 13th May [before O_3 exposure], T1: 11th July [55 days exposure], and T2: 8th September [114 days exposure]). Leaf gas exchange rates were measured using a portable photosynthesis measurement system (LI-6800, Li-Cor instruments, Lincoln, NE, USA). Measurements were carried out between 8 and 12 a.m. CET for one to two plants per plot per treatment. For each plant, three to five leaves with 4th to 6th order from the tip of the shoot were targeted. During the measurement, the parameters within the LI-6800 leaf cuvette were established as follows: CO_2 concentration (420 ppm), leaf temperature (25 °C), photosynthetic photon flux density (PPFD, 1500 µmol m^{-2} s^{-1}, utilizing an LED light source of 10% blue and 90% red light), and relative humidity (50%). From these measurements, light-saturated net photosynthetic rate (A_{sat}) and stomatal conductance (g_s) were determined.

A SPAD meter (Konica Minolta, Tokyo, Japan) was utilized to measure leaf greenness as a proxy of chlorophyll content. In addition, a HandyPEA fluorimeter (Hansatech Instruments, Pentney, Norfolk, UK) was used to measure the chlorophyll a fluorescence. In order to measure the chlorophyll a fluorescence, after 40 min of dark adaptation, leaves were subjected to a 1 second saturating pulse of red light (peak wavelength: 650 nm) at an intensity of 3,000 µmol photons m^{-2} s^{-1} to determine the fluorescence yields in the dark (F_0) and those with a saturating pulse (F_m). The maximum quantum yield (F_v/F_m) was calculated as $F_v/F_m = 1 - (F_0/F_m)$.

2.4. Modeling of Stomatal Conductance

In order to estimate stomatal O_3 flux, it is essential to parameterize the g_s model. A measurement campaign of g_s for 4th to 6th ordered leaves of all target plants using an open flow-through differential porometer (LI-600, Lincoln, NE, USA) was conducted. Stomatal conductance was measured on 19 sampling days, scheduled at approximately monthly intervals and covering a range of environmental conditions. The resulting dataset, comprising 593 measurements, was used to parameterize the multiplicative g_s model [24,25], as described below:

$$g_s = g_{max} \cdot f_{light} \cdot max\{f_{min,} (f_{temp} \cdot f_{VPD})\} \quad (2)$$

where g_{max} is the maximum stomatal conductance (mol O_3 m^{-2} Projected Leaf Area [PLA] s^{-1}). All other functions are expressed in relative terms and scaled from 0 to 1. The model incorporates minimum stomatal conductance (f_{min}), and it adjusts gs based on PPFD (f_{light}), temperature (f_{temp}), and vapor pressure deficit (VPD) (f_{VPD}). The details of the model functions are available in the Supplementary file (Appendix Method S1). In this study, the function of soil water content (f_{SWC}) was not included because plants did not receive any soil water stress. The model was parameterized using the boundary line approach [26,27]. The g_{max} and f_{min} values were set as the 95th and 5th percentiles of all g_s data, respectively, following the methodology of Bičárová et al. [28] and Hoshika et al. [25].

2.5. Calculation of Ozone Indices

For daylight periods, identified by shortwave radiation exceeding 50 W m^{-2}, AOT40 was obtained by summing the hourly exceedance of O_3 concentrations above the 40 ppb threshold, following CLRTAP [29]. It is defined as:

$$AOT40 = \sum_{i=1}^{n} max([O_3]_i - 40, 0) \quad (3)$$

 doi:10.20944/preprints202605.0989.v1

where [O_3]i represents the measured hourly O_3 concentration (ppb), with i ranging from 1 to n in the integral, where n is the total number of hours in the calculation period.

According to CLRTAP [29], stomatal O_3 flux (F_{st}; nmol m^{-2} s^{-1}) can be given as:

$$F_{st} = [O_3] \cdot g_s \cdot \frac{r_c}{r_b + r_c} \quad (4)$$

where [O_3] (ppb) is the hourly O_3 concentration, r_c is the surface resistance of leaf (= 1/(g_s + g_{ext}); s m^{-1}), g_s is the cuticular conductance (m s^{-1}), and r_b is the boundary layer resistance of the leaf (s m^{-1}) calculated as r_b = 1.3 ×150 ×(L_d / u) 0.5 where u is the wind speed (m s^{-1}), L_d is the cross-wind leaf dimension (0.05 m for broadleaves, [29]).

POD_Y (mmol m^{-2}) was calculated as the sum of hourly F_{st} data as:

$$POD_Y = \sum_{i=1}^{n} max(F_{st\_i} - Y, 0) \quad (5)$$

where F_{st_i} is the hourly stomatal O_3 uptake (nmol m^{-2} s^{-1}), n is the number of hours included in the calculation period. Y is a species-specific threshold of stomatal O_3 uptake (nmol m^{-2} s^{-1}). In the mapping manual [29], Y = 1 nmol m^{-2} s^{-1} is recommended to assess the negative O_3 effects on woody plant species. Therefore, we utilized POD_1 to establish dose-response relationships with O_3 VFI and physiological parameters.

2.6. Data Analysis

To assess treatment effects, PII and physiological parameters (A_{sat}, g_s, SPAD, and F_v/F_m) were analyzed on absolute values by two-way ANOVA with O_3 treatment and time as fixed factors, including their interaction, after verifying normality and homogeneity of variances. When significant effects were detected ($p \leq 0.05$), differences among levels were evaluated using Tukey's HSD post hoc test.

Dose–response relationships were analyzed separately by expressing each response variable as a relative change from an operational baseline, defined by the mean value measured under AA at T0 (considered as the reference condition in which features were unaffected by O_3). Exposure- and flux-based dose–response functions were then fitted using AOT40 or POD_1 as predictors, comparing (i) a linear model and (ii) a non-linear polynomial model (proposed for O_3 risk assessment applications by Hoshika et al. [30]). Model selection was primarily based on the Akaike Information Criterion (AIC), which balances goodness-of-fit and model complexity; the coefficient of determination (R^2) was used to quantify the proportion of variance explained.

A sensitivity scenario analysis was also conducted to quantify how assumptions on stomatal regulation affect flux-based estimates. Specifically, when AOT40 reached 12 ppm h (as suggested by Gottardini et al. [16]), POD_1 was recalculated under a set of imposed stomatal-closure scenarios (0–50% closure, 10% increments) to simulate additional environmental stress (e.g., drought).

For VFI, CLs were defined as the exposure/uptake at which symptoms first occurred, operationally identified as the point at which PII became > 0 (PII = 0.01). For physiological parameters, the CL was defined as the dose corresponding to a 4% reduction relative to the baseline, following Hoshika et al. [30]. All statistical analyses were performed using OriginPro 2025 (OriginLab Corporation, Northampton, MA).

3. Results

3.1. Ozone Visible Foliar Injury and the Number of Leaves

The first O_3 VFI for the plants treated with 2.0× O_3 exposure were observed after 16 days of exposure (on 14th June). Subsequently, the symptoms emerged in the other two O_3 treatments (i.e., AA and 1.5×) 32 days after the beginning of the exposure (on 2nd July). The O_3 VFI are characterized by interveinal stippling on the adaxial leaf surface, with a reddish to dark brown coloration (Figure 2). These stipples were localized between the veins, often sparing the vein tissue itself, and did not show signs of tissue necrosis or insect damage.

 doi:10.20944/preprints202605.0989.v1

Color-composition analysis identified 16 perceptual colors that captured the main chromatic features of O_3 VFI in *V. lantana* (Figure 2). The selected palette described a gradual shift from light to dark brownish tones, with reddish intermediates, consistent with the visual progression of injury.

The PII was significantly affected by the interaction between treatment and time ($p < 0.05$, Table 1, Table S1). Across all O_3 treatments, PII values increased over time, with O_3 VFI already evident but not statistically significant at T1. At this stage, mean PII values exceeded 1.5 in the two elevated O_3 treatments (2.03 ± 1.11 in 1.5× and 2.12 ± 1.41 in 2.0×), reaching maximum values of 0.61 in AA, 3.83 in 1.5×, and 4.79 in 2.0×. Injury became even more pronounced at T2, with a statistical difference under the 2.0× treatment. At T2, while the AA showed modest increases (mean values were 1.29 ± 0.71), the 1.5× O_3 treatment showed a decrease, justified by leaf senescence in this treatment (1.31 ± 0.62), and a significant rise in PII was observed in the 2.0× treatment at T2 (9.06 ± 3.24). Variability in PII was high across treatments; the lowest PII value was 0.1, recorded in the 1.5× at T1 (i.e., 1.00% of SL and 10% of SA), and the highest recorded value of 14.13 was in 2.0× T2 (i.e., 41.3% of SL and 34.21% of SA).

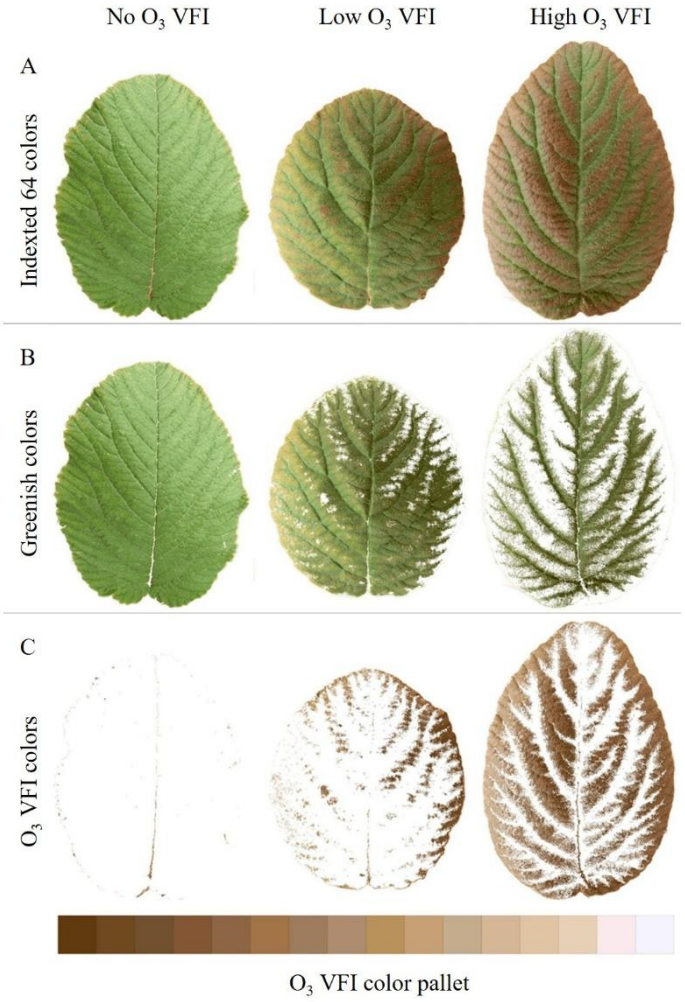

Figure 2. Perceptual color composition of the O_3 VFI (visible foliar injury) in *Viburnum lantana*. The 16 selected colors illustrate the gradient of O_3 VFI development, ranging from light to dark brownish hues (darker colors correspond to higher levels of alteration, indicating more severe damage—e.g., light grey = low damage; dark brown = high damage) with intermediate reddish tones.

3.2. Ozone Effects on Photosynthetic Parameters

The A_{sat} was significantly affected by both treatment ($p < 0.05$) and time ($p < 0.001$) (Table 1, Table S1). Across treatment, a consistent decline was observed from AA to 2.0×, with AA presenting an average A_{sat} of 10.45 ± 1.10 μmol m^{-2} s^{-1}, 1.5× an intermediate value of 9.07 ± 1.09 μmol m^{-2} s^{-1}, and

 doi:10.20944/preprints202605.0989.v1

2.0× an average of 8.16 ± 1.38 μmol m^{-2} s^{-1}. Across time, A_{sat} at T1 (7.81 ± 0.45 μmol m^{-2} s^{-1}) and T2 (6.34 ± 0.76 μmol m^{-2} s^{-1}) were statistically lower than the baseline (T0: 13.54 ± 0.53 μmol m^{-2} s^{-1}).

Regarding the g_s, there was only a statistically significant influence of time ($p < 0.0001$) (Table 1, Table S1), with mean values decreased from 0.172 ± 0.014 mol m^{-2} s^{-1} at T0 to 0.091 ± 0.007 mol m^{-2} s^{-1} at T1 and remained at a similar level at T2 (0.091 ± 0.006 mol m^{-2} s^{-1}).

SPAD values, indicative of relative chlorophyll content, were significantly affected by the O_3 treatment ($p < 0.05$, Table 1, Table S1). Across all timepoints, the AA plants showed the highest mean SPAD values (50.42 ± 1.76), which were significantly higher than those observed in the 1.5× treatment (42.22 ± 2.12). In contrast, the 2.0× treatment group exhibited intermediate SPAD values (42.82 ± 6.62), which did not differ significantly from either AA or 1.5× due to the high within-group variability.

F_v/F_m was significantly affected by the interaction between treatment and time ($p < 0.01$; Table 1, Table S1). Across all three O_3 treatments, F_v/F_m values remained stable throughout the experiment, with mean values of 0.72 ± 0.01, indicating limited temporal variation in PSII photochemical efficiency. A notable exception, however, was observed in the 2.0× treatment, which showed a significant decrease in F_v/F_m during mid-summer (T1: 0.64 ± 0.01), followed by a recovery at T2. This transient reduction was not observed at the other two exposure levels, which maintained consistent F_v/F_m values across all time points.

Table 1. Plant Injury Index (PII) and physiological traits measured (light-saturated net photosynthetic rate [A_{sat}], stomatal conductance [g_s], SPAD, the maximum photochemical efficiency of PSII [Fv/Fm]) in *Viburnum lantana* sampling under ambient air (AA), 1.5×AA, and 2.0×AA O_3 treatments. Measurements were taken before exposure (T0, 13th May), after 55 days (T1, 11th July) and after 114 days (T2, 8th September). Values are reported as plot means ± SE (n = 3). Significance levels from two-way ANOVA are indicated as *** $p \leq 0.001$, ** $p \leq 0.01$, * $p \leq 0.05$, and —= not significant. Different letters denote significant differences among O_3 and time interactions based on Tukey's HSD test.

O_3 × Time		PII	A_{sat} μmol m^{-2} s^{-1}	g_s μmol m^{-2} s^{-1}	SPAD	F_v/F_m
T0	AA	0.00 ± 0.00^a	14.68 ± 1.03	0.20 ± 0.03	44.40 ± 1.15	0.75 ± 0.00^a
	1.5×	0.00 ± 0.00^a	13.08 ± 0.75	0.14 ± 0.01	43.77 ± 1.37	0.73 ± 0.01^a
	2.0×	0.00 ± 0.00^a	12.85 ± 0.91	0.17 ± 0.01	40.43 ± 3.17	0.75 ± 0.01^a
T1	AA	0.44 ± 0.12^a	8.05 ± 0.22	0.07 ± 0.00	52.10 ± 0.64	0.73 ± 0.01^a
	1.5×	2.03 ± 1.11^a	7.47 ± 1.13	0.10 ± 0.01	39.90 ± 3.55	0.71 ± 0.02^a
	2.0×	2.12 ± 1.41^a	7.92 ± 1.02	0.10 ± 0.01	41.27 ± 5.78	0.64 ± 0.01^b
T2	AA	1.29 ± 0.71^a	8.62 ± 0.32	0.09 ± 0.01	54.77 ± 2.54	0.74 ± 0.01^a
	1.5×	1.31 ± 0.62^a	6.68 ± 0.65	0.10 ± 0.01	42.97 ± 5.49	0.75 ± 0.02^a
	2.0×	9.06 ± 3.24^b	3.73 ± 0.60	0.08 ± 0.02	46.77 ± 5.20	0.72 ± 0.01^a
ANOVA	O_3	*	**	–	*	**
	Time	**	***	***	–	**
	O_3 × Time	*	–	–	–	**

3.3. Parameterization of the Stomatal Conductance Model

The g_{max} value found for *V. lantana* was 0.158 mol O_3 m^{-2} PLA s^{-1}, whereas f_{min} was set to 0.06. The limitations of g_s due to environmental factors are shown in Figure 3. With increasing light intensity, a sharp increase in g_s was observed, even under a relatively low PPFD (200 μmol m^{-2} s^{-1}), as shown by f_{light} (f_{light_a} = 0.0163). The optimal temperature for stomatal opening (T_{opt}) was 24 °C, while T_{max} and T_{min} were set to 41 and 0 °C, respectively. In addition, a high air VPD observed in the afternoon caused stomatal closure, as confirmed by the f_{VPD} function (VPD_{max}: 1.8 kPa, VPD_{min}: 6.4 kPa).

 doi:10.20944/preprints202605.0989.v1

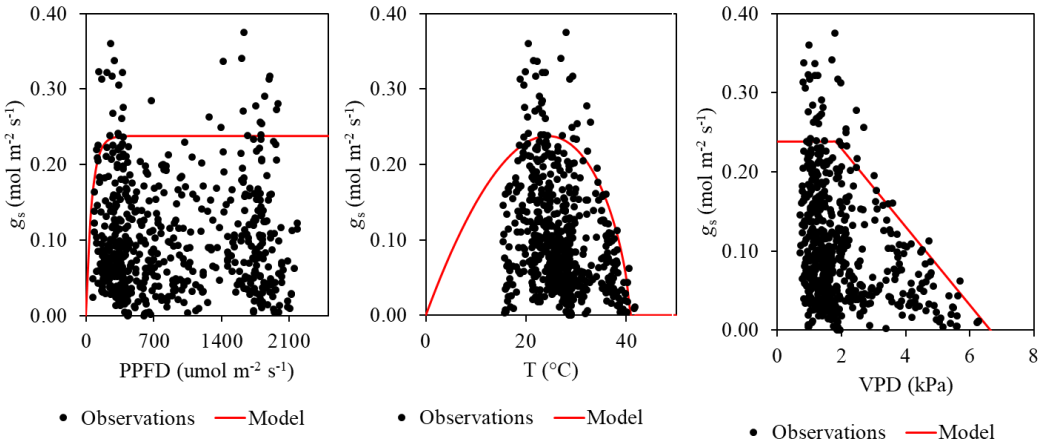

Figure 3. Parameterization of stomatal response functions (f_{light}, f_{temp}, and f_{VPD}) for *Viburnum lantana*. The fitted stomatal response functions are shown as red curves, with measured stomatal conductance values (g_s) plotted as black points.

3.4. The Relation of O_3 Indices, Plant Injury Index (PII), and Plant Physiological Responses

The results of the linear and polynomial regression models examining the relationships between PII and the physiological parameters (A_{sat}, g_s, SPAD, and F_v/F_m) and the two indices (POD_1 and AOT40) showed varying levels of model fit and explanatory power (Table S2). All the regressions were statistically significant except for SPAD and F_v/F_m, thus will not be discussed in the study.

For the PII, the polynomial model performed better than the linear one, and the AOT40 (Figure 4A inset) performed slightly better than POD_1 (Figure 4A). As it was clear that the PII response remained flat across time of exposure and then sharply rose over a narrow interval at the end of the exposure period, we considered both polynomial models (with AOT40 and POD_1) as suitable for representing the species response (Figure 4A).

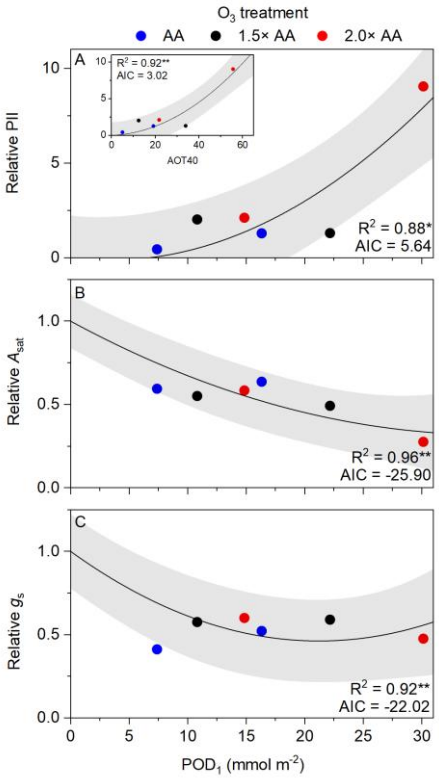

 doi:10.20944/preprints202605.0989.v1

Figure 4. Regression models between the selected features of *Viburnum lantana*: (**A**) Relative Plant Injury Index (PII), (**B**) Relative light-saturated net photosynthetic rate (A_{sat}), (**C**) Relative stomatal conductance (g_s) and ozone exposure metrics (Phytotoxic Ozone Dose above a threshold of 1 nmol m^{-2} s^{-1}—POD_1 (**A–C**) or the Accumulated Ozone Exposure Over a Threshold of 40 ppb—AOT40 [A-inset]. Each graph reports the regression line, corresponding coefficient of determination (R^2), and Akaike Information Criterion (AIC). Statistical significance of the regression is indicated as: ** $p \leq 0.01$, * $p \leq 0.05$.

The best-fit model for physiological parameters was the polynomial, performed with POD_1 (Figure 4 B,C). The A_{sat} declined rapidly at low POD_1, then approached a stable lower plateau at higher POD_1. However, A_{sat} remained well below its initial level across the higher POD_1 values, especially at the end of the exposure period, indicating reduced leaf photosynthetic capacity with increasing accumulated O_3 uptake (Figure 4B).

For g_s, the polynomial function using POD_1 also provided the best fit, showing a lower AIC compared to all the other tested functions (Table S2). The fitted curve was similar to that for A_{sat}, with g_s decreasing sharply at low POD_1, then stabilizing, when g_s had already declined substantially from its initial levels, and continued to decrease gradually as POD_1 increased (Figure 4C).

3.5. Critical Levels

The exposure- or flux-based CLs were calculated for all significant regressions (Table S2), and Table 2 reports only the CLs of the chosen best-fit functions.

Comparing the CLs calculated for the PII, the values were considerably higher with the polynomial function (7.82 mmol m^{-2} for POD_1 and 4.42 ppm h for AOT40, Table 2) than with the linear regressions (0.54 mmol m^{-2} for POD_1 and 0.81 ppm h for AOT40; Table S2).

In contrast, for the physiological parameters, the polynomial fits produced lower CLs than the linear fits, and g_s consistently showed lower CLs than A_{sat}, indicating an earlier response of stomatal conductance to O_3 (POD_1: 1.22 vs 1.61 mmol m^{-2}; AOT40: 1.31 vs 2.27 ppm h, respectively; Table 2).

Table 2. Ozone critical levels (CLs) for visible foliar injury and physiological responses in *Viburnum lantana* were estimated through the Plant Injury Index (PII), light-saturated net photosynthetic rate (A_{sat}), and stomatal conductance (g_s). Two metrics of ozone exposure were examined and tested using the polynomial model: the stomatal flux-based Phytotoxic Ozone Dose above a threshold of 1 nmol m^{-2} s^{-1} (POD_1), and the exposure-based AOT40 (Accumulated Ozone Exposure Over a Threshold of 40 ppb). The CLs for PII were calculated considering the injury onset (PII = 0.01), and for the photosynthetic parameters were derived as 4% reduction from the baseline value.

Variable / O_3 index	AOT40 (ppm h)	POD_1 (mmol m^{-2})
PII	4.42	7.82
A_{sat}	2.27	1.61
g_s	1.31	1.22

4. Discussion

The manipulative experimental approach adopted in our study for the first time enabled the following new findings on O_3 effect on both O_3 VFI and the physiological features of the important bioindicator species, *V. lantana*, filling a significant knowledge gap regarding the integrated response of the species to O_3 stress.

4.1. Validation of Ozone Visible Foliar Injury Based on Free-Air Experiments

The appearance and progression of O_3 VFI observed in *V. lantana* under elevated O_3 treatments confirmed that this species is sensitive to O_3 exposure. Plants exposed to 2.0× developed VFI two weeks earlier than those at lower treatment levels, following a clear dose-dependent pattern. This observation aligns with previous experimental studies on O_3 VFI for this species, which found that

 doi:10.20944/preprints202605.0989.v1

higher AOT40 levels were associated with more frequent VFI [23]. Previous studies suggest that the onset timing of O_3 VFI shows species-specific dependency; for instance, the O_3-sensitive deciduous species, *Alnus glutinosa* and *Vaccinium myrtillus*, showed early-season symptom development, whereas the O_3-tolerant Mediterranean shrub, *Arbutus unedo*, exhibited a delayed onset of O_3 VFI, appearing only in the late growing season [11,15,31]. In our study, although the O_3 VFI onset was found in the early summer, PII values at 2.0× treatment became significantly higher than in the AA treatment only at T2, likely reflecting the slow development of O_3 damage in *V. lantana* throughout the growing season.

The symptoms consisted of small reddish-brown spots distributed on the upper leaf surface, mainly in the interveinal areas. Veins were generally unaffected, and the leaves did not show necrotic patches or damage patterns attributable to insects or pathogens [11]. The color analysis (Figure 2) supported this pattern, showing a chromatic gradient from light grey to dark brown, indicative of increasing tissue alteration, similar to the colors observed in previous field assessments [17,31]. These colorimetric patterns not only reflect the severity of foliar damage but may also serve as a diagnostic tool for O_3 injury under field conditions. As demonstrated by Moura et al. [15], the color components observed in experimental manipulations are comparable in many species to those detected in field samples, confirming the comparability between controlled and natural environments. This suggests that the color profiles documented in our study could be effectively used for quality control and support field-based O_3 VFI assessments, enhancing the accuracy of visual diagnosis in biomonitoring applications.

Despite the clear development of O_3 VFI, the correspondence with systemic eco-physiological responses was only partial, highlighting the complexity of O_3–plant interactions. While PII increased significantly with O_3 exposure and A_{sat} showed a marked decline, the response of g_s was more limited. The decrease of A_{sat} in the absence of g_s reduction in O_3-exposed leaves was similarly found in Japanese Siebold's beech [32] and I-214 poplar clone [33]. Since the rates of damage to photosynthesis and stomatal conductance do not always coincide, O_3 exposure can decouple g_s from A_{sat} [25,34]. In fact, O_3 impairs stomatal function, leading to reduced stomatal responsiveness to environmental stimuli, i.e., stomatal sluggishness [35,36]. The remaining open stomata reduce water-use efficiency, increasing the risk of other climate crisis factors, such as drought [37].

In our study, this partial decoupling between O_3 VFI and physiological impairment may be linked to 'invisible' damage and physiological modifications, including repair processes, before visible signs of injury appear [38]. A recent study applied Terahertz (THz) imaging analysis and revealed that the negative effect of O_3 on leaf water status was associated with cell damage before the onset of VFI in *Carpinus betulus* L. and *Ostrya carpinifolia* Scop. plants [39]. In fact, in our experiment, the marked reduction in A_{sat} was already found at T1, even though PII was still relatively low. Moreover, a significant decline in F_v/F_m was observed at 2.0× only at the early time point (T1), suggesting an initial impairment of PSII photochemical efficiency. The absence of sustained effects at later stages may indicate a partial recovery over time or a localized, non-systemic damage response. Similar dynamics were reported by Bussotti et al. [40] in a field-based study on *V. lantana*, in which chlorophyll fluorescence measurements under high O_3 exposure showed a marked reduction in parameters related to electron transport efficiency. These converging observations confirm the moderate physiological sensitivity of *V. lantana* to O_3, with photochemical alterations detectable even before O_3 VFI becomes widespread, consistent with findings from both field and controlled studies.

4.2. Flux-Based Assessment of Ozone Visible Injury and Physiological Parameters

This study also aimed to evaluate whether O_3-induced effects on *V. lantana* are better captured by the flux-based index (POD_1) rather than the exposure-based index (AOT40). Regression analyses confirmed that POD_1 was a superior metric for capturing the physiological response, with the polynomial model fitting better than the linear regression, specifically, for A_{sat} and g_s. While both O_3 indices were significantly related to PII, the polynomial model with POD_1 again showed a tendency toward a better fit and better represented the biological process (Figure 4A inset, Table S2).

 doi:10.20944/preprints202605.0989.v1

The stronger association between POD_1 can be attributed to its physiological basis. Unlike exposure-based metrics such as AOT40, which rely solely on ambient O_3 concentrations, POD_1 estimates the actual O_3 dose absorbed through stomata. This flux-based approach is widely recognized as the primary driver of O_3-induced phytotoxicity [4,6], as it accounts for plant-specific factors such as stomatal regulation under varying environmental conditions (e.g., water availability). Furthermore, we recommend using non-linear models for dose-response relationships, as emphasized by Hoshika et al. [30], particularly when they outperform linear regression.

4.3. Critical Levels

The use of the PII offers an integrated measure of O_3 VFI damage by combining both the proportion of symptomatic leaves per plant (SL) and the average affected area within those leaves (SA). This dual-component approach provides a more realistic representation of total O_3 VFI than frequency-based metrics alone. In our study, we proposed that the CL for PII should be calculated when the PII value reaches 0.1, indicating the onset of damage (i.e., 1% SL and 10% SA), which, in the case of *V. lantana*, using the polynomial regression as the best fit (Table S2), occurred when POD_1 reached 7.82 mmol m^{-2} (Table 2).

If calculated using the exposures-based index AOT40, the polynomial regression fit better, and the CL for the PII was determined to be 4.42 ppm h. In the past, a threshold of 12 ppm h was proposed for the species to indicate injury onset based on field observations in the Mediterranean Alps [18]. The discrepancy between the calculated CL presented here and previous literature may result from differences in environmental conditions affecting stomatal O_3 uptake between natural forests and the FO_3X experimental facility. In fact, during summer-time, drought often limits stomatal O_3 uptake for trees at the natural forest sites in the Mediterranean Alps (–31% due to soil water deficit, [14]), whereas, at the FO_3X, plants were well-irrigated and any water stress was not expected to reduce g_s for *V. lantana* and thus enhancing stomatal O_3 uptake. A sensitivity analysis revealed that, if the 30% hypothetical stomatal closure occurred at the FO_3X, the values of POD_1 at the field-observed threshold 12 ppm h AOT40 would be 5.9 to 9.9 mmol m^{-2}, which agrees with the flux-based CL (7.82 mmol m^{-2}) (Table S3). The results indicate that the AOT40-based CL may vary across the target regions due to insufficient consideration of the biological processes underlying O_3 uptake. Given that stomata are the primary interface for O_3 entry into plants, a stomatal flux-based approach should be recommended for a proper setting of CL in forest protection against O_3 pollution.

Interestingly, although a flux-based POD_1 CL for PII was identified as 7.82 mmol m^{-2} POD_1, physiological thresholds for a 4% reduction in A_{sat} and g_s were observed at lower POD_1 values (1.61 mmol m^{-2} and 1.22 mmol m^{-2}, respectively). This suggests that physiological alterations begin before the manifestation of visible injury, supporting the use of combined indicators for a comprehensive assessment. Therefore, a multi-indicator framework combining morphological and physiological indicators is recommended to detect early stress signals and assess cumulative O_3 impact more accurately [41]. This approach improves detection sensitivity, enhances inter- and intra-species comparisons in biomonitoring, and underscores the importance of flux-based metrics in O_3 risk assessment. Low POD values as CLs for physiological parameters were also found in other sensitive species, where the CLs for A_{sat} were suggested to be 1.9 to 3.5 mmol m^{-2} POD_0 for O_3-sensitive deciduous poplars and hornbeam species [39]; therefore, *V. lantana* can be identified as a sensitive species to O_3.

5. Conclusions

This study examined O_3 effects on *V. lantana* under open-air experimental conditions. Results showed a dose-dependent pattern, with O_3 VFI appearing first in plants exposed to a higher O_3 environment (2.0× treatment). These visual injuries matched field symptoms and were confirmed by colorimetric analysis.

At the same time, physiological responses revealed a more complex pattern. While A_{sat} and F_v/F_m declined under elevated O_3, g_s and SPAD were less responsive, suggesting that physiological

 doi:10.20944/preprints202605.0989.v1

alterations can occur with a different pattern. Notably, thresholds for a 4% reduction in A_{sat} and g_s were reached at POD_1 levels below those needed to induce VFI, highlighting the importance of combining visual and functional indicators to avoid underestimating damages. The dose–response analysis also showed that the flux-based metric POD_1 better explained variability in physiological parameters than the exposure-based AOT40, supporting the actual consensus that stomatal uptake is a more accurate predictor of plant damage. Thus, we suggested CLs of 1.61 mmol m^{-2} and 1.22 mmol m^{-2} POD_1 for A_{sat} and g_s, respectively, and a CL of 7.82 mmol m^{-2} for the onset of O_3 VFI.

In conclusion, this study provides the first detailed eco-physiological characterization of the O_3 effect in *V. lantana* under controlled and realistic exposure conditions. It confirms the species' moderate sensitivity to O_3 and refines critical thresholds for O_3 risk assessment. *V. lantana* is confirmed as an auspicious bioindicator for integrated O_3 impact monitoring, particularly when physiological and morphological parameters complement visual assessments.

Supplementary Materials: The following supporting information can be downloaded at the website of this paper posted on Preprints.org, Method S1: Model functions of stomatal conductance model; Table S1. Two-way ANOVA test on physiological parameters, Table S2. Regression models evaluating the relation between Plant Injury Index (PII) and the physiological parameters, Table S3. Sensitivity analysis of POD_1.

Author Contributions: Elena Marra: Writing—original draft, Investigation, Formal analysis, Validation, Conceptualization. Barbara Baesso Moura: Writing—review & editing, Formal analysis, Validation. Elena Paoletti: Writing—review & editing, Conceptualization, Resources, Project administration. Andrea Viviano: Writing—review & editing, Investigation. Jacopo Manzini: Writing—review & editing, Investigation. Ryoji Tanaka: Writing—review & editing. Yasutomo Hoshika: Conceptualization, Resources, Project administration, Investigation, Supervision. All authors have read and agreed to the published version of the manuscript.

Funding: This study was supported by Fondazione Cassa di Risparmio di Firenze (2013/7956), LIFE project AIRFRESH (LIFE19 ENV/FR/000086) and MODERn NEC (LIFE20GIE / IT / 000091) of the European Commission, @CNR project 4ClimAir (SAC.AD002.173.019), PNRR for Mission 4 (Component 2, Notice 3264/2021, IR0000032)—ITINERIS—Italian Integrated Environmental Research Infrastructure System CUP B53C22002150006; and Project funded under the National Recovery and Resilience Plan (NRRP), Mission 4 Component 2 Investment 1.4—Call for tender No. 3138 of 16 December 2021, rectified by Decree n.3175 of 18 December 2021 of Italian Ministry of University and Research funded by the European Union—NextGenerationEU, Award Number: Project code CN_00000033, Concession Decree No. 1034 of 17 June 2022 adopted by the Italian Ministry of University and Research, CUP, H43C22000530001 Project title "National Biodiversity Future Center—NBFC" (Spoke 3 and 5).

Data Availability Statement: All raw datasets generated or analyzed in this study can be provided by the corresponding author upon reasonable request.

Acknowledgments: We thank Alessandro Materassi, Gianni Fasano, and Francesco Sabatini for maintenance of the ozone FACE; Moreno Lazzara and Leonardo Lazzara for support during field work.

Conflicts of Interest: The authors declare no conflicts of interest.

Abbreviations

The following abbreviations are used in this manuscript:

AA	Ambient air
AIC	Akaike Information Criterion
ANOVA	Analysis of variance
AOT40	Accumulated Ozone Exposure Over a Threshold of 40 ppb
A_{sat}	Light-saturated net photosynthetic rate
CET	Central European Time
CL	Critical level
CLRTAP	Convention on Long-range Transboundary Air Pollution

 doi:10.20944/preprints202605.0989.v1

CNR	National Research Council of Italy
DOY	Day of year
EEA	European Environment Agency
FACE	Free-Air Controlled Exposure
FO_3X	Free-air O3 eXposure facility
F_0	Minimum fluorescence yield in dark-adapted leaves
F_m	Maximum fluorescence yield after a saturating light pulse
F_{st}	Stomatal ozone flux
F_v/F_m	Maximum photochemical efficiency of photosystem II
g_{ext}	External or cuticular conductance
g_{max}	Maximum stomatal conductance
g_s	Stomatal conductance
HSD	Honestly significant difference
ICP Forests	International Co-operative Program on Assessment and Monitoring of Air Pollution Effects on Forests
LED	Light-emitting diode
NBFC	National Biodiversity Future Center
NRRP	National Recovery and Resilience Plan
O_3	Ozone
PII	Plant Injury Index
PLA	Projected leaf area
POD_1	Phytotoxic Ozone Dose above a threshold of 1 nmol m^{-2} s^{-1}
POD_Y	Phytotoxic Ozone Dose above a flux threshold of Y nmol m^{-2} s^{-1}
PPFD	Photosynthetic photon flux density
PSII	Photosystem II
R^2	Coefficient of determination
*r*b	Boundary layer resistance
*r*c	Surface resistance of leaf
RGB	Red, green, blue color model
ROS	Reactive oxygen species
SA	Percentage of affected area on symptomatic leaves
SE	Standard error
SL	Percentage of symptomatic leaves per plant
SLA	Specific leaf area
SPAD	Soil Plant Analysis Development leaf color index, used as a proxy for chlorophyll content
SWC	Soil water content
T0	Time zero, before ozone exposure
T1	First measurement time, 55 days exposure
T2	Second measurement time, 114 days exposure
THz	Terahertz
T_{max}	Maximum temperature parameter for stomatal response
T_{min}	Minimum temperature parameter for stomatal response
*T*opt	Optimum temperature for stomatal opening
Treat.	Treatment
UNECE	United Nations Economic Commission for Europe
VFI	Visible foliar injury
VPD	Vapor pressure deficit

References

1. European Environment Agency Assessment of Ground-Level Ozone in EEA Member Countries, with a Focus on Long-Term Trends; Publications Office: LU, 2009;
2. Mills, G.; Pleijel, H.; Malley, C.S.; Sinha, B.; Cooper, O.R.; Schultz, M.G.; Neufeld, H.S.; Simpson, D.; Sharps, K.; Feng, Z.; et al. Tropospheric Ozone Assessment Report: Present-Day Tropospheric Ozone Distribution and Trends Relevant to Vegetation. *Elementa: Science of the Anthropocene* **2018**, *6*, 47, doi:10.1525/elementa.302.

 doi:10.20944/preprints202605.0989.v1

3. Vollenweider, P.; Ottiger, M.; Günthardt-Goerg, M.S. Validation of Leaf Ozone Symptoms in Natural Vegetation Using Microscopical Methods. *Environmental Pollution* **2003**, *124*, 101–118, doi:10.1016/S0269-7491(02)00412-8.
4. Paoletti, E. Ozone Impacts on Forests. *CABI Reviews* **2007**, doi:10.1079/PAVSNNR20072068.
5. Dusart, N.; Gandin, A.; Vaultier, M.-N.; Joffe, R.; Cabané, M.; Dizengremel, P.; Jolivet, Y. Importance of Detoxification Processes in Ozone Risk Assessment: Need to Integrate the Cellular Compartmentation of Antioxidants? *Front. For. Glob. Change* **2019**, *2*, 45, doi:10.3389/ffgc.2019.00045.
6. Grulke, N.E.; Heath, R.L. Ozone Effects on Plants in Natural Ecosystems. *Plant Biol J* **2020**, *22*, 12–37, doi:10.1111/plb.12971.
7. Moura, B.B.; Alves, E.S. Climatic Factors Influence Leaf Structure and Thereby Affect the Ozone Sensitivity of Ipomoea Nil 'Scarlet O'Hara.' *Environmental Pollution* **2014**, *194*, 11–16, doi:10.1016/j.envpol.2014.06.042.
8. Lefohn, A.S.; Malley, C.S.; Smith, L.; Wells, B.; Hazucha, M.; Simon, H.; Naik, V.; Mills, G.; Schultz, M.G.; Paoletti, E.; et al. Tropospheric Ozone Assessment Report: Global Ozone Metrics for Climate Change, Human Health, and Crop/Ecosystem Research. *Elementa: Science of the Anthropocene* **2018**, *6*, 27, doi:10.1525/elementa.279.
9. Paoletti, E.; Sicard, P.; Hoshika, Y.; Fares, S.; Badea, O.; Pitar, D.; Popa, I.; Anav, A.; Moura, B.B.; De Marco, A. Towards Long-Term Sustainability of Stomatal Ozone Flux Monitoring at Forest Sites. *Sustainable Horizons* **2022**, *2*, 100018, doi:10.1016/j.horiz.2022.100018.
10. Sicard, P.; De Marco, A.; Carrari, E.; Dalstein-Richier, L.; Hoshika, Y.; Badea, O.; Pitar, D.; Fares, S.; Conte, A.; Popa, I.; et al. Epidemiological Derivation of Flux-Based Critical Levels for Visible Ozone Injury in European Forests. *J. For. Res.* **2020**, *31*, 1509–1519, doi:10.1007/s11676-020-01191-x.
11. Schaub, M.; Calatayud, V.; Ferretti, M.; Brunialti, G.; Lövblad, G.; Krause, G.; Sanz, M.J. Part VIII: Monitoring of Ozone Injury. In *Manual on Methods and Criteria for Harmonized Sampling, Assessment, Monitoring and Analysis of the Effects of Air Pollution on Forests*; Thünen Institute of Forest Ecosystems, Eberswalde, 2016; Vol. 85.
12. Sicard, P.; De Marco, A.; Dalstein-Richier, L.; Tagliaferro, F.; Renou, C.; Paoletti, E. An Epidemiological Assessment of Stomatal Ozone Flux-Based Critical Levels for Visible Ozone Injury in Southern European Forests. *Science of The Total Environment* **2016**, *541*, 729–741, doi:10.1016/j.scitotenv.2015.09.113.
13. Sicard, P.; Hoshika, Y.; Carrari, E.; De Marco, A.; Paoletti, E. Testing Visible Ozone Injury within a Light Exposed Sampling Site as a Proxy for Ozone Risk Assessment for European Forests. *J. For. Res.* **2021**, *32*, 1351–1359, doi:10.1007/s11676-021-01327-7.
14. Marra, E.; De Marco, A.; Ebone, A.; Ferrara, A.M.; Giannetti, F.; Tagliaferro, F.; Sicard, P.; Popa, A.; Popa, I.; Paoletti, E.; et al. Flux-Based Assessment of Ozone Visible Foliar Injury in Southern Alps. *J. For. Res.* **2025**, *36*, 124, doi:10.1007/s11676-025-01918-8.
15. Baesso Moura, B.; Carrari, E.; Dalstein-Richier, L.; Sicard, P.; Leca, S.; Badea, O.; Pitar-Silaghi, D.; Shashikumar, A.; Ciriani, M.-L.; Paoletti, E.; et al. Bridging Experimental and Monitoring Research for Visible Foliar Injury as Bio-Indicator of Ozone Impacts on Forests. *Ecosyst Health Sustain* **2022**, *8*, 2144466, doi:10.1080/20964129.2022.2144466.
16. Gottardini, E.; Cristofori, A.; Cristofolini, F.; Bussotti, F.; Ferretti, M. Responsiveness of Viburnum Lantana L. to Tropospheric Ozone: Field Evidence under Contrasting Site Conditions in Trentino, Northern Italy. *J. Environ. Monit.* **2010**, *12*, 2237, doi:10.1039/c0em00299b.
17. Gottardini, Elena Risposte Morfologiche, Fisiologiche e Geniche All'ozono Della Specie Arbustiva Viburnum Lantana L. PhD thesis, Università degli Studi di Firenze, 2012.
18. Gottardini, E.; Cristofolini, F.; Cristofori, A.; Ferretti, M. Ozone Risk and Foliar Injury on Viburnum Lantana L.: A Meso-Scale Epidemiological Study. *Science of The Total Environment* **2014**, *493*, 954–960, doi:10.1016/j.scitotenv.2014.06.041.
19. Gottardini, E.; Cristofolini, F.; Ferretti, M. Foliar Symptoms on Viburnum Lantana Reflect Annual Changes in Summer Ozone Concentration in Trentino (Northern Italy). *Ecological Indicators* **2017**, *78*, 26–30, doi:10.1016/j.ecolind.2017.02.043.

 doi:10.20944/preprints202605.0989.v1

20. Faralli, M.; Cristofolini, F.; Cristofori, A.; Ferretti, M.; Gottardini, E. Leaf Trait Plasticity and Site-Specific Environmental Variability Modulate the Severity of Visible Foliar Ozone Symptoms in Viburnum Lantana. *PLoS ONE* **2022**, *17*, e0270520, doi:10.1371/journal.pone.0270520.
21. Paoletti, E.; Materassi, A.; Fasano, G.; Hoshika, Y.; Carriero, G.; Silaghi, D.; Badea, O. A New-Generation 3D Ozone FACE (Free Air Controlled Exposure). *Science of The Total Environment* **2017**, *575*, 1407–1414, doi:10.1016/j.scitotenv.2016.09.217.
22. Paoletti, E.; Ferrara, A.M.; Calatayud, V.; Cerveró, J.; Giannetti, F.; Sanz, M.J.; Manning, W.J. Deciduous Shrubs for Ozone Bioindication: Hibiscus Syriacus as an Example. *Environmental Pollution* **2009**, *157*, 865–870, doi:10.1016/j.envpol.2008.11.009.
23. Calatayud, V.; Cerveró, J.; Sanz, M.J. Foliar, Physiologial and Growth Responses of Four Maple Species Exposed to Ozone. *Water Air Soil Pollut* **2007**, *185*, 239–254, doi:10.1007/s11270-007-9446-5.
24. JARVISt, P.G. The Interpretation of the Variations in Leaf Water Potential and Stomatal Conductance Found in Canopies in the Field.
25. Hoshika, Y.; Fares, S.; Pellegrini, E.; Conte, A.; Paoletti, E. Water Use Strategy Affects Avoidance of Ozone Stress by Stomatal Closure in Mediterranean Trees—A Modelling Analysis. *Plant Cell & Environment* **2020**, *43*, 611–623, doi:10.1111/pce.13700.
26. Braun, S.; Schindler, C.; Leuzinger, S. Use of Sap Flow Measurements to Validate Stomatal Functions for Mature Beech (Fagus Sylvatica) in View of Ozone Uptake Calculations. *Environmental Pollution* **2010**, *158*, 2954–2963, doi:10.1016/j.envpol.2010.05.028.
27. Hoshika, Y.; Paoletti, E.; Omasa, K. Parameterization of Zelkova Serrata Stomatal Conductance Model to Estimate Stomatal Ozone Uptake in Japan. *Atmospheric Environment* **2012**, *55*, 271–278, doi:10.1016/j.atmosenv.2012.02.083.
28. Bičárová, S.; Sitková, Z.; Pavlendová, H.; Fleischer, P.; Fleischer, P.; Bytnerowicz, A. The Role of Environmental Factors in Ozone Uptake of Pinus Mugo Turra. *Atmospheric Pollution Research* **2019**, *10*, 283–293, doi:10.1016/j.apr.2018.08.003.
29. CLRTAP Mapping Critical Levels for Vegetation, Chapter III. In Manual on Methodologies and Criteria for Modelling and Mapping Critical Loads and Levels and Air Pollution Effects, Risks and Trends; Geneva, Switzerland, 2017.
30. Hoshika, Y.; Moura, B.B.; Cotrozzi, L.; Nali, C.; Alfarraj, S.; Rennenberg, H.; Paoletti, E. An Assessment of Ozone Risk for Date Palm Suggests That Phytotoxic Ozone Dose Nonlinearly Affects Carbon Gain. *Environmental Pollution* **2024**, *342*, 123143, doi:10.1016/j.envpol.2023.123143.
31. Novak, K.; Skelly, J.M.; Schaub, M.; Kräuchi, N.; Hug, C.; Landolt, W.; Bleuler, P. Ozone Air Pollution and Foliar Injury Development on Native Plants of Switzerland. *Environmental Pollution* **2003**, *125*, 41–52, doi:10.1016/S0269-7491(03)00085-X.
32. Yamaguchi, M.; Watanabe, M.; Iwasaki, M.; Tabe, C.; Matsumura, H.; Kohno, Y.; Izuta, T. Growth and Photosynthetic Responses of Fagus Crenata Seedlings to O3 under Different Nitrogen Loads. *Trees* **2007**, *21*, 707–718, doi:10.1007/s00468-007-0163-x.
33. Hoshika, Y.; Paoletti, E.; Pisuttu, C.; Cotrozzi, L.; Haworth, M.; Pellegrini, E.; Nali, C.; Ribeiro, R.V.; Mayer, J.L.S.; Moura, B.B. Leaf Phenology Determines the Response of Poplar Genotypes to O_3 through Mesophyll Conductance. *The Plant Journal* **2025**, *121*, e70091, doi:10.1111/tpj.70091.
34. Lombardozzi, D.; Sparks, J.P.; Bonan, G.; Levis, S. Ozone Exposure Causes a Decoupling of Conductance and Photosynthesis: Implications for the Ball-Berry Stomatal Conductance Model. *Oecologia* **2012**, *169*, 651–659, doi:10.1007/s00442-011-2242-3.
35. Paoletti, E. Ozone Slows Stomatal Response to Light and Leaf Wounding in a Mediterranean Evergreen Broadleaf, Arbutus Unedo. *Environmental Pollution* **2005**, *134*, 439–445, doi:10.1016/j.envpol.2004.09.011.
36. Hoshika, Y.; De Carlo, A.; Baraldi, R.; Neri, L.; Carrari, E.; Agathokleous, E.; Zhang, L.; Fares, S.; Paoletti, E. Ozone-Induced Impairment of Night-Time Stomatal Closure in O3-Sensitive Poplar Clone Is Affected by Nitrogen but Not by Phosphorus Enrichment. *Science of The Total Environment* **2019**, *692*, 713–722, doi:10.1016/j.scitotenv.2019.07.288.

 doi:10.20944/preprints202605.0989.v1

37. Hoshika, Y.; Katata, G.; Deushi, M.; Watanabe, M.; Koike, T.; Paoletti, E. Ozone-Induced Stomatal Sluggishness Changes Carbon and Water Balance of Temperate Deciduous Forests. *Sci Rep* **2015**, *5*, 9871, doi:10.1038/srep09871.
38. Agrawal, S.B.; Agrawal, M.; Singh, A. *Tropospheric Ozone A Hazard for Vegetation and Human Health*; Cambridge Scholars Publishing, 2021;
39. Pagano, M.; Hoshika, Y.; Gennari, F.; Manzini, J.; Marra, E.; Viviano, A.; Paoletti, E.; Sultana, S.; Tredicucci, A.; Toncelli, A. Probing Ozone Effects on European Hornbeam (Carpinus Betulus L. and Ostrya Carpinifolia Scop.) Leaf Water Content through THz Imaging and Dynamic Stomatal Response. *Science of The Total Environment* **2024**, *956*, 177358, doi:10.1016/j.scitotenv.2024.177358.
40. Bussotti, F.; Agati, G.; Desotgiu, R.; Matteini, P.; Tani, C. Ozone Foliar Symptoms in Woody Plant Species Assessed with Ultrastructural and Fluorescence Analysis. *New Phytologist* **2005**, *166*, 941–955, doi:10.1111/j.1469-8137.2005.01385.x.
41. Bussotti, F.; Pollastrini, M. Observing Climate Change Impacts on European Forests: What Works and What Does Not in Ongoing Long-Term Monitoring Networks. *Front. Plant Sci.* **2017**, *8*, 629, doi:10.3389/fpls.2017.00629.